Molecular Imaging of Reductive Coupling Reactions: Interstitial-Mediated Coupling of Benzaldehyde on Reduced TiO_2(110)

Lauren Benz,[†] Jan Haubrich,[‡] Stephen C. Jensen,[‡] and Cynthia M. Friend[‡,§,*]

[†]Department of Chemistry and Biochemistry, University of San Diego, San Diego, California 92110, United States, [‡]Department of Chemistry and Chemical Biology and [§]School of Engineering and Applied Sciences, Harvard University, Cambridge, Massachusetts 02138, United States

ABSTRACT We report the first visualization of a reactive intermediate formed from coupling two molecules on a surface—a diolate formed from benzaldehyde coupling on TiO_2(110). The diolate, imaged using scanning tunneling microscopy (STM), is reduced to gaseous stilbene upon heating to ~400 K, leaving behind two oxygen atoms that react with reduced Ti interstitials that migrate to the surface, contrary to the popular expectation that strong bonds in oxygenated molecules react only with oxygen vacancies at the surface. Our work further provides both experimental and theoretical evidence that Ti interstitials drive the formation of diolate intermediates. Initially mobile monomers migrate together to form paired features, identified as diolates that bond over two adjacent five-coordiante Ti atoms on the surface. Our work is of broad importance because it demonstrates the possibility of imaging the distribution and bonding configurations of reactant species on a molecular scale, which is a critical part of understanding surface reactions and the development of surface morphology during the course of reaction.

KEYWORDS: scanning tunneling microscopy · density functional theory · titanium dioxide · benzaldehyde · interstitial · oxygen vacancy

Imaging individual reactive intermediates is a long-sought goal in molecular sciences because direct visualization of structure provides insight into bonding and reactivity. While there are many examples of the imaging of individual molecules, reactive coupling has not yet been observed. Herein, we report for the first time the visualization of molecular pairing that produces an intermediate in a C=C bond forming reaction: the coupling of two benzaldehyde molecules to form a diolate on the rutile TiO_2(110) surface. The combination of scanning tunneling microscopy (STM) and density functional theory (DFT) is used illustrate the importance of reduced titanium interstitials in the bonding of benzaldehyde monomers and the formation of the coupling intermediate, the diolate.

Titanium dioxide has been widely studied because of its use in a variety of applications—dye-sensitized solar cells,[1] waste purification,[2] heterogeneous catalysis,[3] sensing,[4,5] coatings,[6,7] and in biocompatible materials[8]—which depend strongly on surface chemistry.[9] Titania is a "reducible" oxide, meaning that oxygen loss from both the surface and the bulk is relatively facile. The activity of reduced TiO_2 toward reaction with oxygenates is often attributed to surface oxygen vacancies.[9,10] However, both surface and bulk defects can contribute to reductive processes. Bulk reduction also alters the optical properties of the titania, clearly signified by the change from transparent to blue in color with the introduction of n-doping color centers.[11] Defects include O vacancies, Ti interstitials, and Ti vacancies, the predominant defect present under reducing conditions being the Ti interstitials.[12,13]

Interstitial reduced titanium centers have the potential to alter the thermal chemistry and photochemistry of TiO_2 surfaces. For example, interstitials are important in the reoxidation of reduced TiO_2(110) at elevated temperatures,[14−19] and a recent scanning tunneling microscopy study imaged morphological changes attributed to reaction of O_2 with interstials.[20] Titanium interstitials have also recently been shown to react with various molecules containing oxygen, including organic acids,[16] aldehydes,[21,22] and NO_2,[23] over the (110) surface. For example, decomposition of formic acid on reconstructed TiO_2(110)-(1 × 2) produces (1 × 1) islands on the (1 × 2) terraces after heating to 470 K[16] when oxygen from the acid reacts with interstitials. We also recently attributed the reductive self-coupling reactions of acrolein[21] and benzaldehyde[22] over TiO_2(110) to interstitials,

*Address correspondence to cfriend@seas.harvard.edu.

Received for review July 31, 2010 and accepted December 28, 2010.

Published online January 13, 2011
10.1021/nn103144u

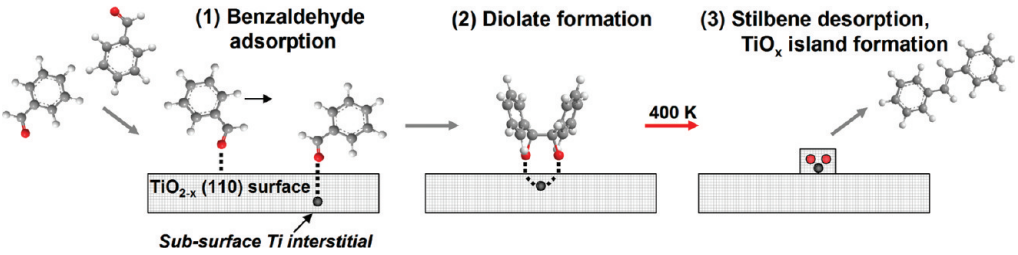

Figure 1. Schematic of benzaldehyde adsorption followed by pairing to form a diolate above a Ti interstitial site. Heating to 400 K produces gaseous stilbene and two oxygen atoms. The oxygen atoms form new nanoscale islands of TiO_x from reaction with titanium interstitials.

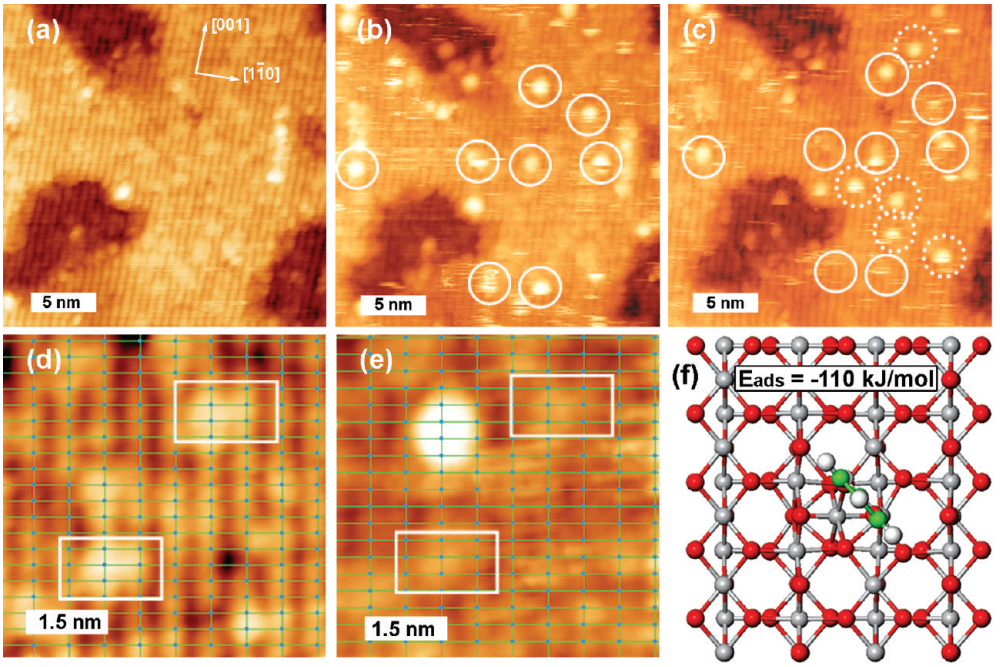

Figure 2. STM images show the mobility of benzaldehyde at low coverages on TiO_2(110) at 300 K. Images of (a) the clean, reduced TiO_2(110) surface; (b) the same region after deposition of 0.01 monolayers (ML) of benzaldehyde at 300 K; and (c) a similar image as in (b) after a ~4 min delay. The benzaldehyde molecules (circled) are mobile at room temperature. High-resolution STM images of (d) clean TiO_2(110) and (e) the same area after benzaldehyde deposition at 300 K (0.01 ML). The white rectangles indicate the positions of two vacancies, and a green lattice grid is shown to guide the eye (lattice points are approximate in the [001] direction). The benzaldehyde molecules are centered over Ti_{5c} rows. (f) Lowest energy structure for benzaldehyde stabilized by a Ti interstitial on TiO_2(110) as calculated using DFT. Oxygen atoms are in red, titanium in gray, carbon in green, and hydrogen in white.

based on observed reactivity and the formation of nanoscale TiO_2 islands after loss of oxygen from benzaldehyde to form stilbene.

The coupling of benzaldehyde over reduced TiO_2(110) was used to image a bimolecular reaction on a molecular scale using scanning tunneling microscopy and to further probe the role of titanium interstitials in this process. The overall reactive process deduced from our studies involves facile diffusion of monomeric benzaldehyde after adsorption at 300 K and subsequent formation of a diolate intermediate that ultimately yields stilbene and TiO_x nanostructures (Figure 1). Contrary to expectations, there is no preference for reaction with oxygen vacancies on the surface. Complementary theoretical calculations show that interstitials play an important role in the formation of the diolate. This reaction is highly (100%) selective—stilbene is the only product so that no carbon or other impurities deposit on the surface—making it ideal for molecular imaging of the reaction. Furthermore, the phenyl ring is imaged readily because of the π-system in the ring, making monomers and dimers readily distinguishable in STM. This work establishes the feasibility of imaging reactive intermediates in synthetic coupling reactions on surfaces—a major advance for investigating complex surface chemistry.

RESULTS AND DISCUSSION

Adsorption of Benzaldehyde Monomers at Room Temperature. At low coverage and at room temperature, benzaldehyde monomers bind on the Ti rows; however, they are mobile under these conditions in STM images (Figure 2). Defects and Ti rows on the clean surface (Figure 2a,d) are used as markers in the images of

benzaldehyde. Oxygen vacancy defects are marked with white rectangles, and a lattice of five-fold coordinated Ti (Ti_{5c}) sites is overlaid to guide the eye (Figure 2d). On clean TiO_2(110), step heights of 3.2 ± 0.4 Å are measured, in accordance with the rutile structure,[24] and alternating bright and dark rows separated by ~6.5 Å that are characteristic of Ti_{5c} and bridging O atom rows, respectively,[25] are observed. The faint bright spots which appear between Ti_{5c} rows on the pristine surface are oxygen vacancy defects, present at a concentration of ~5% relative to the density of Ti_{5c} sites (5.2×10^{14} sites/cm^2), which is within the expected range of ~4−10% for similar surface preparation.[25]

New mobile features, attributed to benzaldehyde monomers, are observed following deposition of benzaldehyde at room temperature (Figure 2b,c,e). The circled round features attributed to benzaldehyde have apparent heights of 3.5 ± 0.4 Å and widths of 1.2 ± 0.1 nm (full width at half-maximum), similar to that of benzaldehyde on Si(100)-(2 × 1) which measures ~1 nm in diameter in STM.[26] The extremely low benzaldehyde coverage in these images, ~0.01 ML, was achieved by imaging during benzaldehyde deposition, so that the tip shadows the nearby region of the surface from gas, requiring that molecules diffuse into the imaging window to be observed. The mobility of benzaldehyde at 300 K is consistent with the fact that a significant fraction of benzaldehyde desorbs at 340 K in temperature-programmed desorption.[22]

An image of the same area, taken ~4 min later, shows that the round features attributed to benzaldehyde move under these conditions (Figure 2c). The solid white circles in Figure 2c indicate the positions of the molecules as they were in Figure 2b, while the dotted white circles indicate the appearance of new features. Some new molecules appear, while others no longer occupy the positions marked with the solid circles, clearly showing that the molecules are mobile on the surface. Furthermore, the streaks observed in the images are consistent with rapid diffusion relative to the time scale of the scanning and possible tip−molecule interactions.

The round features associated with benzaldehyde imaged at this low coverage and relatively short time after adsorption at 300 K are centered on Ti_{5c} rows, which is consistent with either an η^1-atop configuration (bound through the O) on Ti_{5c} sites or, possibly, the dioxyalkylene structure. Either of these structures is possible, based on the combination of STM and DFT, as discussed below; however, the η^1-atop configuration (Figure 2f) is deemed more likely because the dioxyalkylene structure would be less symmetrically disposed over the Ti_{5c} rows because the phenyl ring tilts toward an oxygen row (Figure 3c). Furthermore, the η^1-atop configuration is similar to structures proposed for other oxygenates.[27] The observation of round features on Ti rows provides strong evidence for an atop geometry, in which the aldehydic oxygen interacts electrostatically with the Ti_{5c} center, analogous to proposed bonding geometry of acetone[27,28] and formaldehyde.[29,30] The individual benzaldehyde features circumscribe at least three Ti atoms based on STM images (Figure 2e), suggesting that benzaldehyde is rotating rapidly relative to the imaging time scale of ~240 s, in agreement with the DFT calculations. Other organics containing heteroatoms—catechol,[31] pyridine, and dimethylpyridine[32]—also bind predominantly over the Ti rows on TiO_2(110).

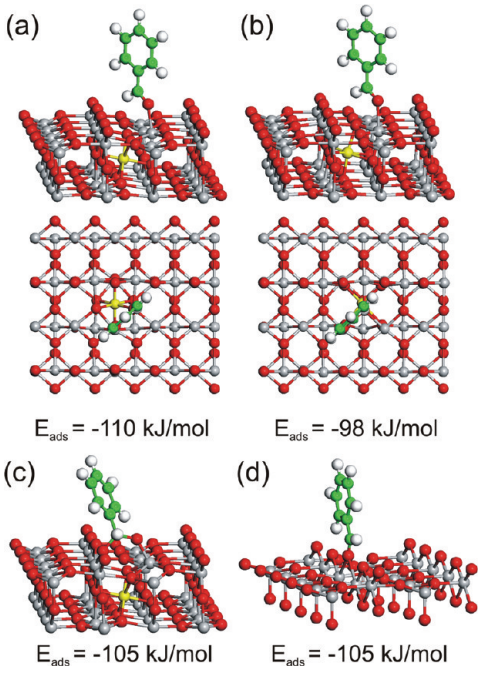

Figure 3. Optimized adsorption benzaldehyde structures and their corresponding binding energies on a defective 5 × 2-TiO_2(110) slab. The four lowest energy configurations are shown, all of which involve Ti interstitials: (a) η^1-atop configuration with molecular plane diagonal to the [001] direction of the rows and a type I interstitial in ⟨110⟩ channel below shown from the side and the top; (b) η^1-atop configuration (diagonal) stabilized by a type II interstitial between two ⟨110⟩ channels (top and side view shown); (c) η^2-dioxyalkylene structure with involvement of a bridging oxygen atom, stabilized by a type I interstitial; (d) η^1-benzaldehyde bonded in a bridging oxygen vacancy site, molecular plane parallel to the [001] direction. Red balls represent O, gray Ti in the lattice, yellow Ti interstitials, green C, and white H atoms.

The adsorption energies obtained from DFT provide evidence that binding of benzaldehyde monomers over defect sites is energetically favored over any binding configuration on the stoichiometric surface (Table 1). On the perfectly stoichiometric surface, the most stable structure has a lone pair of the aldehydic oxygen pointing toward the Ti_{5c} site and the molecular plane rotated diagonally to the rows (Supporting Information Figure S1). The adsorption energy of −86 kJ/mol is substantially weaker than structures involving various defects but stronger than that of the corresponding

TABLE 1. Calculated Adsorption Energies of Benzaldehyde on Stoichiometric and Defective 5 × 2 × 4 Unit Cell[a]

			TiO_2 slab with I_{Ti} between 1st−2nd trilayer	
binding configuration/slab	stoichiometric TiO_2	TiO_2 with BOV (1/10 ML)	I_{Ti} in ⟨110⟩ channel site	I_{Ti} between two channels
η^1-atop/Ti_{5c}, diagonal to rows	−86		**−110**	**−98**
η^1-atop/Ti_{5c}, orthogonal	−85			
η^1-atop/Ti_{5c}, parallel	−78			
η^2-dioxyalkylene with Ti_{5c}/O_{br}	−66		**−105**	−74
η^1/BOV, parallel		**−105**		
η^1/BOV, orthogonal		−79		
η^1-atop/Ti_{5c}, diagonal to rows, near BOV		−74		

[a] All energies are given in kJ/mol. Energies that are in bold have structures given in Figure 3. Other structures are in Supporting Information, Figures S1 and S2. I_{Ti} = "Ti interstitial".

formaldehyde structure (−69 kJ/mol),[33] indicating an electronic contribution of the ring to the interaction with the surface. Nevertheless, this is weakly bound compared to those structures involving reduced Ti centers. The effect of interstitials on binding is comparable for benzaldehyde and formaldehyde,[33] which suggests that also for benzaldehyde the stabilization may be strongly dependent on the distance to the interstitial site and very local in nature.

There are three binding configurations associated with defects that are essentially the same energy: η^1-atop configuration over a Ti_{5c} site with an interstitial Ti below (−110 kJ/mol), η^1 bound to a BOV (−105 kJ/mol), and the η^2-dioxyalkylene (−105 kJ/mol) (Figure 3, Table 1). The η^1-atop binding over a Ti_{5c} site with an interstitial Ti between the ⟨110⟩ channels is also similar in energy, 98 kJ/mol. Clearly, reduction of TiO_2 leads to surface and subsurface defects that can stabilize the adsorption of molecules, including benzaldehyde, through a combination of electron transfer[34] and surface relaxation.[35] Point defects between the first and second layers were investigated in order to obtain upper bounds for the stabilization effects of subsurface defects. The effect is comparable to that of formaldehyde[33] which suggests that also for benzaldehyde the stabilization may be strongly dependent on the distance to the interstitial site and very local in nature. If the diffusion barrier of benzaldehyde along the five-coordinated Ti rows is in the typical range of 10−30% of its adsorption energy,[36] the molecules should readily diffuse to the interstitial sites at room temperature, as is observed.

None of the round features in our STM experiments were centered over oxygen vacancy sites or over the bridging O rows (Figure 2d,e), which clearly shows that binding over BOV sites is not prevalent. Although energetically as stable as the interstitial stabilized configurations within the systematic DFT error, the adsorption structure in a BOV (Figure 3d) was not observed.

The lack of benzaldehyde binding to bridging oxygen vacancies is **not** due to blockage of these sites with water or OH. First, directional dosing was employed, and a base pressure in the 10^{-11} Torr range was maintained before and after dosing (compared to pressures of *ca.* 2×10^{-10} Torr during dosing), thus, minimizing water exposure. Second, vacancy defects appeared uniform in size and brightness even after benzaldehyde exposure, as opposed to the varying size and brightness one expects from single and double hydroxyl formation upon water dissociation.[37] Furthermore, purposeful exposure to water does not alter surface reactivity toward benzaldehyde.[22] However, we cannot completely rule out that coverage and temperature effects may play a role in determining the occupation sequence (population) of the different types of defect sites.

One possible explanation for the lack of benzaldehyde adsorption in surface vacancies could be that there is a kinetic barrier for the diffusion of benzaldehyde from the Ti_{5c} sites into vacancy sites. For example, a recent study of O_2 dissociation on reduced TiO_2(110) found that oxygen adatoms on Ti_{5c} sites can be stable at room temperature in the presence of nearby vacancies, which also points to a significant activation barrier.[38] Indeed, preliminary studies of formaldehyde using DFT indicate that there is a barrier for diffusion into a BOV site, although refinement of the calculation is necessary.

The η^2-dioxyalkylene structure stabilized by Ti interstitials (Figure 3c) is also possible based on the DFT calculations. This structure cannot be unequivocally ruled out, although it would be expected to be asymmetrically positioned with respect to the Ti_{5c} rows, based on the ring tilt. Rotation of the ring toward the other oxygen row on the time scale of the imaging experiments would make this asymmetry undetectable. Hence, we cannot rule out this species. Indeed, it may be a pathway for migration from one Ti_{5c} row to the next.

Diolate Formation from Reaction of Benzaldehyde at Higher Coverages. Reaction of benzaldehyde to form the precursor to reductive coupling is observed at higher coverages of benzaldehyde. The fact that these features

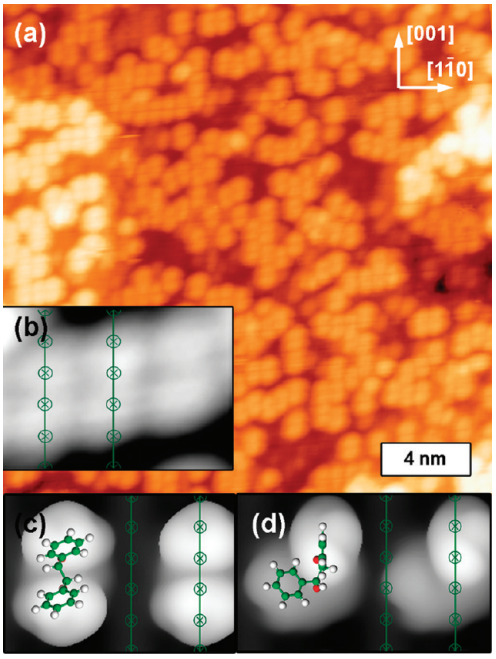

Figure 4. Formation of diolates *via* benzaldehyde pairing is observed using STM. (a) Low-temperature STM image of benzaldehyde adsorption over TiO_2(110) taken at 50 K. (b) Image of a 21 Å × 14 Å group of paired features. The green overlay shows the underlying Ti lattice. (The position of the Ti atoms is not exact in the [001] direction, but the spacing is correct.) The contrast is enhanced in (b) for comparison to (c), the simulated image of the lowest energy *trans*-diolate structure on the same size scale, and (d) the simulated image of the higher energy *cis*-diolate. In both cases, the diolates are on two adjacent Ti_{5c} sites. The simulations are for constant−current images of empty state (+0.5 to 0 eV above the theoretical "Fermi" level (corresponding to $U_{bias} \approx 0.5$ V) and a tip−sample distance of ~4 Å using the Tersoff−Hamann[66] approach. The two measured lobes correspond to the charge density of the two phenyl rings in the simulated images, providing a qualitative guide. Both simulations include an interstitial below between two ⟨110⟩ channel sites (lowest energy configuration). Red balls represent O, gray Ti, green C, and white H atoms. Additional simulations are included in the Supporting Information, Figure S4. Image acquired with a sample bias voltage of 1.9 V and a constant tunneling current of 0.11 nA.

are also observed during *in situ* scanning at 300 K establishes that a covalent interaction binds them together. A weakly bound van der Waal's complex would not persist under these conditions. The dispersion interaction should contribute less than 0.2 eV, using benzene dimerization, which has an energy of 0.12 eV without zero-point correction,[39] as a reference. Oblong features attributed to formation of the diolate intermediate from two benzaldehyde molecules are clearly visible after depositing ~0.2 ML benzaldehyde at 25 K, subsequently heating to ~350 K, cooling and imaging at 50 K (Figure 4a,b). The diolate intermediate also forms at 300 K over a time span of *ca.* 120 min for a coverages of 0.1 ML or above (Supporting Information, Figure S3). In these images, lone diolates are clearly discerned from longer chains observed at higher coverages.

The diolates form over the entire surface, **not** preferentially at surface bridging oxygen vacancies, and are always centered on the five-coordinate Ti rows. We never observed diolates between Ti_{5c} rows in an exhaustive search of thousands of features over ~25 μm^2 at different scanning temperatures and tunneling conditions. Thus, it is clear that the precursor to reductive coupling does not selectively form at *surface* bridging oxygen vacancy sites. Diolates orient along the [001] direction with a faint node-like depression between the two lobes. These features were stationary over the duration of scanning (~5 h), which provides further evidence that they are covalently attached. If, instead, there were weak forces leading to simple packing of benzaldehyde, feature sizes of random multiples, rather than dimers would form. Instead, discrete pairs were observed by STM which formed over Ti atom rows (Figure 4a,b and Figure S3 in the Supporting Information). The apparent length along the [001] direction is measured to be 1.1 ± 0.1 nm, and the measured height was 1.6 ± 0.2 Å.

Going across the [1$\bar{1}$0] direction, a single feature averaged 5.5 ± 0.6 Å in width, slightly less than the spacing between Ti rows of ~6.5 Å. This overall decrease in apparent size and change in shape in comparison to the singular mobile features shown in Figure 2 may be due to a number of factors: (1) upon pairing, the molecules are no longer mobile or rotating; (2) the orientation of the rings is diagonal to the rows, giving the elongated shape; and (3) there may be a change in electronic structure upon pairing. The distance between the two lobes of each feature is 3.5 ± 0.3 Å, which is slightly larger than the 3 Å spacing between the Ti atoms in the [001] direction and in agreement with the DFT calculations. The average experimentally measured distance between pairs which stacked in the [1$\bar{1}$0] direction was 7.1 ± 0.7 Å, slightly larger than the distance between Ti rows (6.5 Å). In counting each elongated feature as two benzaldehyde molecules, we estimated the coverage to be 0.2 ML.

The bonding of these paired intermediates and the corresponding STM images were modeled using DFT. Preliminary X-ray photoelectron spectroscopy (XPS) studies provide evidence that the C−O bond remains intact after heating to 300 K (Supporting Information, Figure S5); therefore, the diolate structures were used to model the paired species (Figure 4c,d). The diolate structure is similar to that proposed previously for reductive coupling on highly reduced Ti(001), although others have proposed that stilbene forms rapidly at 300 K.[40,41] On TiO_2(110), a diolate was proposed to form from two formaldehyde molecules adsorbed in adjacent oxygen vacancies.[42]

The formation of the diolates on two adjacent Ti_{5c} sites by coupling of the aldehydic carbons with a new C−C bond leads to a substantial energy gain compared

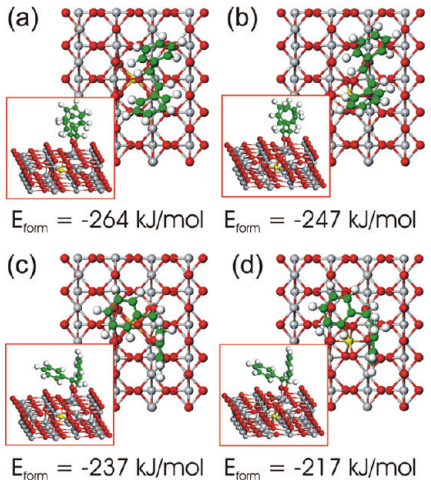

Figure 5. Optimized adsorption structures and corresponding binding energies of *trans*- and *cis*-diolates (a,b and c,d, respectively) on a 5 × 2-TiO_2(110) slab with two different types of subsurface Ti interstitials (a and c with type I interstitial in ⟨110⟩ channel; b and d with type II interstitial between two channels) using the DFT-PW91 calculations. These structures were used to simulate STM images (Figure 4c,d and Supporting Information Figure S4). Red balls represent O, gray Ti in the lattice, yellow Ti interstitials, green C, and white H atoms.

TABLE 2. Calculated Formation Energies of Diolates from Two Gas-Phase Benzaldehyde Molecules on the Defective 5 × 2 × 4 TiO_2 Slab[a]

	TiO_2 slab with I_{Ti} between 1st−2nd trilayer	
binding configuration/slab	I_{Ti} in ⟨110⟩ channel site	I_{Ti} between two channels
(s)-*trans*-diolate	−247	**−264**
(s)-*cis*-diolate	−217	−237

[a] All energies are given in kJ/mol. I_{Ti} = "Ti interstitial".

to the adsorption of two molecules (Figure 5, Table 2). Compared to the lowest energy η^1 configuration (E_{ads} = −110 kJ/mol), up to 44 kJ/mol additional energy can be gained with the most stable *trans*-diolate structure above an interstitial site between ⟨110⟩ channels (Figure 5a).

The formation of these diolates *requires* the involvement and stabilization by Ti interstitials. Both interstitial types I and II stabilize both the both *cis*- and *trans*-diolates, but the symmetric positioning in a type II site in the center below the diolates is generally favored by *ca.* 20 kJ/mol, which is above the DFT error bar. The diolate formed with a new C−C bond between two adjacent benzaldehyde molecules is stable in the presence of subsurface interstitials but not on a stoichiometric slab. Diolates adsorbed next to each other in bridging oxygen vacancies are also stable in our calculations (not shown); however, this structure disagrees with the features centered over the Ti_{5c} rows as observed in STM. We speculate that the kinetic barriers involved in the diffusion of separate BOVs, or, respectively, molecules bonded in BOVs, and subsequent coupling are higher and disfavor this pathway. Corresponding investigations of the different coupling pathways are underway for a simpler probe, formaldehyde. A preliminary estimate of the barrier for coupling of two adjacent *formaldehyde* molecules is ∼51 kJ/mol. The diolates would most likely form upon diffusion of a second benzaldehyde molecule to one that is bonded on a Ti_{5c} site over a subsurface interstitial.

Of the four possible isomers of the diolate structures, the *trans*-configuration bound over a type I interstitial (in the ⟨110⟩ channel) is the most stable (Figure 4c and Figure 5a). The other structures, most notably the *cis* isomers, are considerably less stable (Figure 5, Table 2). Furthermore, only the *trans* isomer structures agree with our STM images (Figure 4), whereas the *cis* isomers do not (Figure 4d and Figure S4 in Supporting Information). Bonding to two adjacent five-coordinate Ti sites, they shadow four Ti_{5c} sites along their long axis, consistent with the length of the two lobes of an intermediate of 900 pm. The simulations for the *cis* isomers show an "L"-shaped feature, that present on the surface should give rise to diastereomeric domains.

Although STM studies of other ring compounds, including benzoic acid[43] and catechol[31] have been reported, the stacking of these phenyl-containing species is different than for the benzaldehyde diolates observed here. Benzoic acid forms benzoate on TiO_2(110), which binds strongly to Ti atoms along the [001] Ti troughs in a bidentate fashion. At 0.5 ML saturation coverage, these bound benzoate molecules then form dimer and trimer rows due to the interaction of the phenyl rings *across* the Ti rows (in the [1$\bar{1}$0] direction)—different than the direction of pairing for benzaldehyde along the [001] direction. The packing of the benzoates is attributed to interactions between phenyl rings because neither acetate[44] nor formate,[45] both lacking this ring, pair on the TiO_2(110) surface. Catechol on TiO_2(110) also preferentially stacks across Ti troughs (in the [001] direction).[31]

The benzaldehyde *diolates* do, however, stack in chains of various lengths *across* the Ti rows, similar to catechol and benzoate. This packing is imperfect in that there is often an offset from the [1$\bar{1}$0] direction between the center of one diolate and the next. This offset measures on average to be 3.4 ± 0.9 Å in the [001] direction, close to the distance of ∼3 Å between unit cells. Although the exact nature of the ring interactions is unclear,[46,47] it is conceivable that the stacking and the offsets observed are the result of noncovalent ring interactions. "T"-type phenyl group interactions were presumed to occur in the case of benzoic acid adsorption on TiO_2(110),[43] with one ring oriented such that the H atoms of the ring are pointed toward the center of the π-ring of the other ring. It is likely that packing of the *trans*-diolates in our experiment

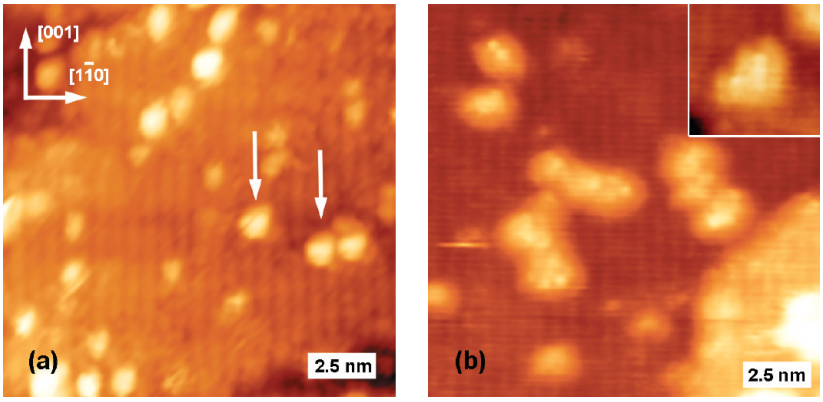

Figure 6. (a) STM image of a TiO_2(110) surface after adsorbing 0.1 ML benzaldehyde and heating to 500 K. (b) STM image of a TiO_2(110) surface after adsorbing 0.3 ML benzaldehyde and heating to 900 K. A nanoscale island with the underlying terrace structure visible is shown in the inset. Both images were acquired at room temperature.

occurs through similar interactions, which we will more generally attribute to van der Waals type interactions,[47] and giving rise to the straight chains and chains with offsets observed. Current DFT methods are not capable of modeling such interactions.

Formation of TiO_2 Nanoscale Islands *via* Benzaldehyde Reduction. Cleavage of the C−O bonds in the diolates upon heating to ~400 K leads to evolution of stilbene and formation of nascent TiO_2 species from reaction of the oxygen lost from the diolate and a Ti interstitial that migrates to the surface (Figure 1).[22] New features attributed to nascent TiO_2 are observed following heating of benzaldehyde ($\theta \sim 0.1$ ML) to 500 K (Figure 6a). As reported previously, gaseous stilbene is evolved below this temperature and no carbon remains on the surface.[22] After heating to 500 K, there are no visible paired features (Figure 6), even though they are clearly observed after adsorption of benzaldehyde at room temperature (Figure S3 in Supporting Information). Instead, few features attributed to nascent TiO_2 particles, indicated by white arrows in the image, appear above the bridging O atom rows. These features measured 4.1 ± 0.8 Å in height and 9.2 ± 2.0 Å in width and are very similar to those reported by Wendt *et al.*,[20] who noted the formation of new terraces following exposure of a reduced TiO_2(110) surface to oxygen. Further deposition of a total of 0.3 ML and annealing to 900 K produced larger, more ordered features that clearly have the characteristic row structure of TiO_2(110) (Figure 6b). The inset shows one feature which exhibits the underlying row structure, demonstrating that deposition of benzaldehyde followed by annealing leads to the formation of nanoscale TiO_2 and TiO_x terraces. As reported previously, after annealing to 900 K, these new terraces measure 3.4 ± 0.9 Å in height, consistent with the step height of 3.2 Å, and 1.6 ± 0.2 nm in width, spanning slightly more than the distance between two Ti rows on average.

SUMMARY

Our unprecedented imaging of diolates formed from benzaldehyde using STM are used in conjunction with DFT to show that benzaldehyde coupling on reduced TiO_2(110) is promoted by subsurface interstitials. The features attributed to the diolate appear as discretely paired features along the rows in the [001] direction and are attributed to the *trans*-diolate configuration based on comparison to simulations using DFT.

Titanium interstitials also bind benzaldehyde monomers more strongly, which provides a mechanism for trapping of a monomer and formation of the diolate. The interstitials drive the ensuing reductive coupling that yields stilbene and nanoscale TiO_2 islands observed using STM. DFT calculations show that reaction with the interstitials is thermodynamically favorable and help identify specific intermediates. Our work also provides further evidence of the importance and highly dynamic nature of subsurface interstitials in surface redox chemistry and points to the controllable nanostructuring of TiO_2 by reaction with an organic over layer.

METHODS

Scanning tunneling microscopy (STM) experiments were performed at room temperature and at 50 K using liquid He cooling with a variable temperature Omicron STM (VT-STM/AFM model) in a chamber with a base pressure of ~3×10^{-11} Torr. All images were acquired in constant current mode, with a sample−tip bias of 1.6 to 2.2 V and a tunneling current of 0.07−0.40 nA, such that electrons tunneled into the empty states of the sample. Image processing was done using WSXM.[48] Electrochemically etched W tips were employed. Benzaldehyde was cleaned with repeated freeze−pump−thaw cycles, and cleanliness was checked with a quadrupole mass spectrometer (Pfeiffer Prisma 200) and subsequently dosed through a leak valve coupled to a directional doser which was positioned ~4 cm

in front of the sample. The STM sample was prepared with multiple cycles of sputtering (20 min each cycle, 1 kV, 2 μA total current) and annealing in a separate preparation chamber (~1000 K, 5 min, after each sputter cycle), until reduced to a blue color. We confirmed reactivity for the benzaldehyde coupling reaction using the mass spectrometer. Sample heating was accomplished using a doped silicon wafer mounted directly beneath the sample, and a temperature calibration was separately performed using a type K thermocouple glued into a second sample with ultrahigh vacuum compatible ceramic glue (Aremco, Ceramabond 503). Finally, the chamber also contained an Auger electron spectrometer (Omicron) with which we checked sample cleanliness before and after reaction.

Density functional theory calculations were carried out using the plane wave code implemented the Vienna Ab Initio simulation package.[49,50] We employed PAW pseudopotentials[51] and the well-established GGA-PW91 functional[52] but also performed test calculations using the PBE functional,[53] which as expected did not differ from each other. Since there is substantial controversy as to the accuracy of hybrid functionals and the "appropriate" empirical amount of Hartee−Fock admixture,[54−60] we did presently not pursue calculations with such functionals. Although it is often quoted that DFT-GGA does not reproduce the band gap and gap states due to defects in reducible oxides and semiconductors,[54−57,59,60] we want to point out that, in contrast to time-dependent DFT, ground-state DFT is not a correct technique to compute excited state properties (such as unoccupied states) and the band gap.[61] In contrast, it has been shown that GGA functionals despite their shortcomings give accurate energetics and structural parameters on TiO_2.[54,58,62−65]

In order to model defect concentrations and avoid lateral interactions between more than two benzaldehyde molecules, a 5 × 2 unit cell was modeled with a 4-trilayer thickness and a large vacuum of ~16 Å above. The two uppermost trilayers were relaxed as well as the adsorbates and the defects, while the bottom layers were fixed at the optimized bulk distances. Dipole corrections have been applied normal to the slabs to minimize unphysical interactions between repeating images.

A plane wave cutoff of 400 eV together with Gaussian smearing (0.2 eV) and 1 × 3 × 1 special Monkhorst-Pack k-point meshes[66] were employed. Convergence was tested by systematic increase of the cutoff to 600 eV and the increase of the k-point mesh to 3 × 3 × 1, which resulted or adsorption energy differences below 2 kJ/mol. However, we estimate that the systematic error bar in calculated energies due to the inherent approximation made by the choice of surface cell, coverage, periodicity, GGA functional, and computational parameters (basis set, Fourier grids, smearing methods, plane wave projector pseudopotentials, zero-point vibrational energy, *etc.*) is on the order of 5−10 kJ/mol. The effect of spin has been tested for all calculations, and the low spin solutions (singlet) have been found to be lowest in energy with the GGA functional.[54,55,58,62] However, the use of different functionals may change the relative energy of different spin configurations.[54,55,58,62] For further computational details, please see ref 35. Constant current STM simulations have been carried out within the Tersoff−Hamann approximation,[67] and results have been visualized using the "p4vasp" software.[68] A tip−surface distance of ~4 Å, a U_{bias} of 0.5 eV, and an isocontour value of 1×10^{-4} electrons/Å^3 was chosen for all images, and the density was smoothed with a Gaussian function to qualitatively simulate the effect of a finite sized tip. We note that this bias was chosen in the calculations to best represent the clean surface, allowing a reasonable qualitative comparison to the actual STM images.[63] At tested higher U_{bias} of +1 eV, the contrast between bright Ti rows and dark bridging O rows was reduced, but the unoccupied π states of the phenyl ring still dominated the images. The discrepancy between the experimental and theoretical bias may be partly due to DFT being a ground-state theory (but STM tunneling into virtual states)[69] and the known inaccuracy of DFT-GGA approaches to correctly predict the band gap for TiO_2 and, hence, the position of the Fermi level[62−64,69] which, furthermore, strongly depends on the reduction degree of the surface (see for example work-function changes in ref 35). With respect to the calculations involving Ti interstitials, two configurations were tested: Ti interstitials in ⟨110⟩ channel sites (type I) and in a site between two ⟨110⟩ channels (type II). These two models on an adsorbate-free slab are energetically identical within the DFT error bar (the binding site between two ⟨110⟩ channels is ~2 kJ/mol lower in energy, Figure 3b). This model corresponds to a realistic defect concentration of *ca.* 2.5%[20] for a low coverage of benzaldehyde (0.1 ML) when using a (5 × 2 × 4) slab.

Acknowledgment. The authors gratefully acknowledge support of this work by the Chemistry Division of the National Science Foundation under Award No. CHE-0545335. J.H. acknowledges support through a Feodor-Lynen fellowship of the A. v. Humboldt foundation and thanks the staff of the Odyssey Cluster at the Faculty of Arts and Sciences of Harvard University. S.C.J. thanks NSF for his Graduate Research Fellowship (GRF). We also would like to thank C. M. Elias (REU student) and R. Schalek (staff) for assistance with the STM experiments.

Supporting Information Available: Room temperature STM results, preliminary XPS data, and additional STM simulations. This material is available free of charge *via* the Internet at http://pubs.acs.org.

REFERENCES AND NOTES

1. O'Regan, B.; Grätzel, M. A Low-Cost, High-Efficiency Solar Cell Based on Dye-Sensitized Colloidal TiO_2 Films. *Nature* **1991,** *353*, 737–740.
2. Mills, A.; Davies, R. H.; Worsley, D. Water-Purification by Semiconductor Photocatalysis. *Chem. Soc. Rev.* **1993,** *22*, 417–425.
3. Satterfield, C. N. *Heterogeneous Catalysis in Industrial Practice*; McGraw-Hill: New York, 1991.
4. Dutta, P. K.; Ginwalla, A.; Hogg, B.; Patton, B. R.; Chwieroth, B.; Liang, Z.; Gouma, P.; Mills, M.; Akbar, S. Interaction of Carbon Monoxide with Anatase Surfaces at High Temperatures: Optimization of a Carbon Monoxide Sensor. *J. Phys. Chem. B* **1999,** *103*, 4412–4422.
5. Xu, Y.; Yao, K.; Zhou, X.; Cao, Q. Platinum−Titanium Oxygen Sensors and Their Sensing Mechanisms. *Sens. Actuators, B* **1993,** *14*, 492–494.
6. Selhofer, H.; Muller, R. Comparison of Pure and Mixed Coating Materials for AR Coatings for Use by Reactive Evaporation on Glass and Plastic Lenses. *Thin Solid Films* **1999,** *351*, 180–183.
7. Paz, Y.; Luo, Z.; Rabenberg, A.; Heller, A. Photooxidative Self-Cleaning Transparent Titanium Dioxide Films on Glass. *J. Mater. Res.* **1995,** *10*, 2842–2848.
8. Larsson, C.; Thomsen, P.; Aronsson, B. O.; Rodahl, M.; Lausmaa, J.; Kasemo, B.; Ericson, L. E. Bone Response to Surface-Modified Titanium Implants: Studies on the Early Tissue Response to Machined and Electropolished Implants with Different Oxide Thicknesses. *Biomaterials* **1996,** *17*, 605–616.
9. Diebold, U. The Surface Science of Titanium Dioxide. *Surf. Sci. Rep.* **2003,** *48*, 53–229.
10. Pang, C. L.; Lindsay, R.; Thornton, G. Chemical Reactions on Rutile TiO_2(110). *Chem. Soc. Rev.* **2008,** *37*, 2328–2353.
11. Li, M.; Hebenstreit, W.; Diebold, U.; Tyryshkin, A. M.; Bowman, M. K.; Dunham, G. G.; Henderson, M. A. The Influence of the Bulk Reduction State on the Surface Structure and Morphology of Rutile TiO_2(110) Single Crystals. *J. Phys. Chem. B* **2000,** *104*, 4944–4950.
12. Aono, M.; Hasiguti, R. R. Interaction and Ordering of Lattice Defects in Oxygen Deficient Rutile TiO_{2-x}. *Phys. Rev. B* **1993,** *48*, 12406–12414.
13. Bak, T.; Nowonty, J.; Rekas, M.; Sorrell, C. C. Defect Chemistry and Semiconducting Properties of Titanium Dioxide: II. Defect Diagrams. *J. Phys. Chem. Solids* **2003,** *64*, 1057–1067.
14. Henderson, M. A. Surface Perspective on Self-Diffusion in Rutile TiO_2. *Surf. Sci.* **1999,** *419*, 174–187.
15. Henderson, M. A. Mechanism for the Bulk-Assisted Reoxidation of Ion Sputtered TiO_2 Surfaces: Diffusion of Oxygen

to the Surface or Titanium to the Bulk. *Surf. Sci.* **1995,** *343*, L1156–L1160.
16. Bennett, R. A.; Stone, P.; Smith, R. D.; Bowker, M. Formic Acid Adsorption and Decomposition on Non-stoichiometric TiO_2(110). *Surf. Sci.* **2000,** *454*−*456*, 390–395.
17. Li, M.; Hebenstreit, W.; Gross, L.; Diebold, U.; Henderson, M. A.; Jennison, D. R.; Schultz, P. A.; Sears, M. P. Oxygen-Induced Restructuring of the TiO_2(110) Surface: A Comprehensive Study. *Surf. Sci.* **1999,** *437*, 173–190.
18. Onishi, H.; Iwasawa, Y. Dynamic Visualization of a Metal-Oxide-Surface/Gas-Phase Reaction: Time-Resolved Observation by Scanning Tunneling Microscopy at 800 K. *Phys. Rev. Lett.* **1996,** *76*, 791–794.
19. Stone, P.; Bennett, R. A.; Bowker, M. Reactive Re-oxidation of Reduced TiO_2(110) Surfaces Demonstrated by High Temperature STM Movies. *New J. Phys.* **1999,** *1*, 1.1–1.2.
20. Wendt, S.; Sprunger, P. T.; Lira, E.; Madsen, G. K. H.; Li, Z. S.; Hansen, J. O.; Matthiesen, J.; Blekinge-Rasmussen, A.; Laegsgaard, E.; Hammer, B.; *et al.* The Role of Interstitial Sites in the Ti3d Defect State in the Band Gap of Titania. *Science* **2008,** *320*, 1755–1759.
21. Benz, L.; Haubrich, J.; Quiller, R. G.; Friend, C. M. Acrolein Coupling on Reduced TiO_2(110): The Effect of Surface Oxidation and the Role of Subsurface Defects. *Surf. Sci.* **2009,** *603*, 1010–1017.
22. Benz, L.; Haubrich, J.; Quiller, R. G.; Jensen, S. C.; Friend, C. M. McMurry Chemistry on TiO_2(110): Reductive C═C Coupling of Benzaldehyde Driven by Titanium Interstitials. *J. Am. Chem. Soc.* **2009,** *131*, 15026–15031.
23. Haubrich, J.; Quiller, R. G.; Benz, L.; Liu, Z.; Friend, C. M. *In Situ* Ambient Pressure Studies of the Chemistry of NO_2 and Water on Rutile TiO_2(110). *Langmuir* **2010,** *26*, 2445–2451.
24. Onishi, H.; Iwasawa, Y. Reconstruction of TO_2(110) Surface—STM Study with Atomic-Scale Resolution. *Surf. Sci.* **1994,** *313*, L783–L789.
25. Diebold, U.; Lehman, J.; Mahmoud, T.; Kuhn, M.; Leonardelli, G.; Hebenstreit, W.; Schmid, M.; Varga, P. Intrinsic Defects on a TiO_2(110)(1 × 1) Surface and Their Reaction with Oxygen: A Scanning Tunneling Microscopy Study. *Surf. Sci.* **1998,** *411*, 137–153.
26. Huang, H. G.; Zhang, Y. P.; Cai, Y. H.; Huang, J. Y. Selective Attachment of Benzaldehyde on Si(100)-2 × 1: Structure, Selectivity, and Mechanism. *J. Chem. Phys.* **2005,** *123*, 104702-1–104702-6.
27. Henderson, M. A. Acetone Chemistry on Oxidized and Reduced TiO_2(110). *J. Phys. Chem. B* **2004,** *108*, 18932–18941.
28. Pierce, K. G.; Barteau, M. A. *J. Org. Chem.* **1995,** *60*, 2405.
29. Idriss, H.; Kim, K. S.; Barteau, M. A. Surface-Dependent Pathways for Formaldehyde Oxidation and Reduction on TiO_2(001). *Surf. Sci.* **1992,** *262*, 113–127.
30. Lu, G.; Linsebigler, A.; Yates, J. T. Ti^{3+} Defect Sites on TiO_2(110): Production and Chemical Detection of Active Sites. *J. Phys. Chem.* **1994,** *98*, 11733.
31. Li, S. C.; Wang, J.; Jacobson, P.; Gong, X. Q. Correlation between Bonding Geometry and Band Gap States at Organic−Inorganic Interfaces: Catechol on Rutile TiO_2-(110). *J. Am. Chem. Soc.* **2009,** *131*, 980–984.
32. Suzuki, S.; Yamaguchi, Y.; Onishi, H.; Sasaki, T.; Fukui, K.; Iwasawa, Y. Study of Pyridine and Its Derivatives Adsorbed on a TiO_2(110)-(1 × 1) Surface by Means of STM, TDS, XPS and MD Calculation in Relation to Surface Acid−Base Interaction. *Faraday Trans.* **1998,** *94*, 161–166.
33. Haubrich, J.; Kaxiras, E.; Friend, C. M. The Role of Surface and Subsurface Point Defects for Chemical Model Studies on TiO_2: A First-Principles Theoretical Study of Formaldehyde Bonding on Rutile TiO_2(110). *Chem.—Eur. J.* **2011** in press.
34. Deskins, N. A.; Rousseau, R.; Dupuis, M. Defining the Role of Excess Electrons in the Surface Chemistry of TiO_2. *J. Phys. Chem. C* **2010,** *114*, 5891–5897.
35. Haubrich, J.; Friend, C. M. Personal communication.
36. Seebauer, E. G.; Allen, C. E. Estimating Surface Diffusion Coefficients. *Prog. Surf. Sci.* **1995,** *49*, 265–330.
37. Wendt, S.; Schaub, R.; Matthiesen, J.; Vestergaard, E. K.; Wahlstrom, E.; Rasmussen, M. D.; Thostrup, P.; Molina, L. M.; Laegsgaard, E.; Stensgaard, I.; *et al.* Oxygen Vacancies on TiO_2(110) and Their Interaction with H_2O and O_2: A Combined High-Resolution STM and DFT Study. *Surf. Sci.* **2005,** *598*, 226–245.
38. Du, Y. G.; Deskins, N. A.; Zhang, Z. R.; Dohnalek, Z.; Dupuis, M.; Lyubinetsky, I. Formation of O Adatom Pairs and Charge Transfer Upon O_2 Dissociation on Reduced TiO_2-(110). *Phys. Chem. Chem. Phys.* **2010,** *12*, 6337–6344.
39. Ershova, O. V.; Lillestolen, T. C.; Bichoutskaia, E. Study of Polycyclic Aromatic Hydrocarbons Adsorbed on Graphene Using Density Functional Theory with Empirical Dispersion Correction. *Phys. Chem. Chem. Phys.* **2010,** *12*, 6483–6491.
40. Idriss, H.; Pierce, K. G.; Barteau, M. A. Synthesis of Stilbene from Benzaldehyde by Reductive Coupling on TiO_2(001) Surfaces. *J. Am. Chem. Soc.* **1994,** *116*, 3063–3074.
41. Sherrill, A. B.; Lusvardi, V. S.; Eng, J.; Chen, J. G. G.; Barteau, M. A. NEXAFS Investigation of Benzaldehyde Reductive Coupling To Form Stilbene on Reduced Surfaces of TiO_2-(001). *Catal. Today* **2000,** *63*, 43–51.
42. Qiu, H.; Idriss, H.; Wang, Y.; Wöll, C. Carbon−Carbon Bond Formation on Model Titanium Oxide Surfaces: Identification of Surface Reaction Intermediates by High-Resolution Electron Energy Loss Spectroscopy. *J. Phys. Chem. C* **2008,** *112*, 9828–9834.
43. Guo, Q.; Cocks, I.; Williams, E. M. The Adsorption of Benzoic Acid on a TiO_2(110) Surface Studied Using STM, ESDIAD and LEED. *Surf. Sci.* **1997,** *393*, 1–11.
44. Onishi, H.; Yamaguchi, Y.; Fukui, K.; Iwasawa, Y. Temperature-Jump STM Observation of Reaction Intermediate on Metal-Oxide Surfaces. *J. Phys. Chem.* **1996,** *100*, 9582–9584.
45. Iwasawa, Y.; Onishi, H.; Fukui, K. *In Situ* STM Study of Surface Catalytic Reactions on TiO_2(110) Relevant to Catalyst Design. *Top. Catal.* **2001,** *14*, 163–172.
46. Robertson, J. M. The Measurement of Bond Lengths of Conjugated Molecules of Carbon. *Proc. R. Soc. London* **1951,** *207*, 101–110.
47. Grimme, S. Do Special Noncovalent Pi−Pi Stacking Interactions Really Exist? *Angew. Chem., Int. Ed.* **2008,** *47*, 3430–3434.
48. Horcas, I.; Fernandez, R.; Gomez-Rodriguez, J. M.; Colchero, J.; Gomez-Herrero, J.; Baro, A. M. WSXM: A Software for Scanning Probe Microscopy and a Tool for Nanotechnology. *Rev. Sci. Instrum.* **2007,** *78*, 013705-1–013705-8.
49. Kresse, G.; Hafner, J. *Ab Initio* Molecular Dynamics for Liquid Metals. *J. Phys. Rev. B* **1993,** *47*, 558–561.
50. Kresse, G.; Hafner, J. *Ab Initio* Molecular Dynamics for Open-Shell Transition Metals. *J. Phys. Rev. B* **1993,** *48*, 13115–13118.
51. Kresse, G.; Joubert, D. From Ultrasoft Pseudopotentials to the Projector Augmented-Wave Method. *Phys. Rev. B* **1999,** *59*, 1758–1775.
52. Perdew, J. P.; Wang, Y. Accurate and Simple Analytical Representation of the Electron-Gas Correlation Energy. *Phys. Rev. B* **1992,** *45*, 13244–13249.
53. Perdew, J. P.; Burke, K.; Wang, Y. Generalized Gradient Approximation for the Exchange-Correlation Hole of a Many-Electron System. *Phys. Rev. B* **1996,** *54*, 16533–16539.
54. Ganguglia-Pirovano, M. V.; Hoffman, A.; Sauer, J. Oxygen Vacancies in Transition Metal and Rare Earth Oxides: Current State of Understanding and Remaining Challenges. *Surf. Sci. Rep.* **2007,** *62*, 219–270.
55. Pacchioni, G. Modeling Doped and Defective Oxides in Catalysis with Density Functional Theory Methods: Room for Improvements. *J. Chem. Phys.* **2008,** *128*, 182505-1–182505-10.
56. Labat, F.; Baranek, P.; Domain, C.; Minot, C.; Adamo, C. Density Functional Theory Analysis of the Structural and Electronic Properties of TiO_2 Rutile and Anatase Polytypes: Performances of Different Exchange-Correlation Functionals. *J. Chem. Phys.* **2007,** *126*, 154703-1–154703-12.

57. Islam, M. M.; Bredow, T.; Gerson, A. Electronic Properties of Oxygen-Deficient and Aluminum-Doped Rutile TiO_2 from First Principles. *Phys. Rev. B* **2007,** *76*, 045217-1–045217-9.
58. Finazzi, E.; Di Valentin, C.; Pacchioni, G.; Selloni, A. Excess Electron States in Reduced Bulk Anatase TiO_2: Comparison of Standard GGA, GGA plus U, and Hybrid DFT Calculations. *J. Chem. Phys.* **2008,** *129*, 154113-1–154113-9.
59. Cora, F.; Alfredsson, M.; Mallia, G.; Middlemiss, D. S.; Mackrodt, W. C.; Dovesi, R.; Orlando, R. *Principles and Applications of Density Functional Theory in Inorganic Chemistry II*; Springer-Verlag: Berlin, 2004; Vol. 113.
60. Marsman, M.; Paier, J.; Stroppa, A.; Kresse, G. Hybrid Functionals Applied to Extended Systems. *J. Phys.: Condens. Mater.* **2008,** *20*, 064201-1–064201-9.
61. Kresse, G.; Shishkin, M.; Marsman, M.; Paier, J. Accurate Band Gaps and Dielectric Properties from One-Electron Theories. *J. Phys.: Condens. Mater.* **2008,** *20*, 064203.
62. Kowalski, P. M.; Meyer, B.; Marx, D. Composition, Structure, and Stability of the Rutile TiO_2(110) Surface: Oxygen Depletion, Hydroxylation, Hydrogen Migration, and Water Adsorption. *Phys. Rev. B* **2009,** *79*, 115410-1–115410-16.
63. Minato, T.; Sainoo, Y.; Kim, Y.; Kato, H. S.; Aika, K.; Kawai, M.; Zhao, J.; Petek, H.; Huang, T.; He, W.; *et al.* The Electronic Structure of Oxygen Atom Vacancy and Hydroxyl Impurity Defects on Titanium Dioxide (110) Surface. *J. Chem. Phys.* **2009,** *130*, 124502-1–124502-11.
64. Perron, H.; Vandenborre, J.; Domain, C.; Drot, R.; Roques, J.; Simoni, E.; Ehrhardt, J. J.; Catalette, H. Combined Investigation of Water Sorption on TiO_2 Rutile (110) Single Crystal Face: XPS *vs*. Periodic DFT. *Surf. Sci.* **2007,** *601*, 518–527.
65. Rasmussen, M. D.; Molina, L. M.; Hammer, B. Adsorption, Diffusion, and Dissociation of Molecular Oxygen at Defected TiO_2(110): A Density Functional Theory Study. *J. Chem. Phys.* **2004,** *120*, 988–997.
66. Monkhorst, H. J. Special Points for Brillouin-Zone Integrations. *Phys. Rev. B* **1976,** *13*, 5188–5192.
67. Tersoff, J.; Hamann, D. R. Theory of the Scanning Tunneling Microscope. *Phys. Rev. B* **1985,** *31*, 805–813.
68. Retrieved from http://cms.mpi.univie.ac.at/odubay/p4vasp_site/news.php.
69. Stowasser, R.; Hoffmann, R. What Do the Kohn−Sham Orbitals and Eigenvalues Mean? *J. Am. Chem. Soc.* **1999,** *121*, 3414–3420.